Optics Letters

Enhancing the resolution of a near-eye display with a Pancharatnam–Berry phase deflector

Yun-Han Lee, Tao Zhan, and Shin-Tson Wu*

CREOL, The College of Optics and Photonics, University of Central Florida, Orlando, Florida 32816, USA
*Corresponding author: swu@creol.ucf.edu

We report an electro-optic image shifter to enhance the resolution of display devices with a Pancharatnam–Berry phase deflector (PBD). The switching time of our PBD is less than 1 ms. Through synchronizing and computational factorization, we are able to double the display resolution for reducing the screen door effect. Such a thin and lightweight PBD image shifter can be easily integrated into wearable display devices. Its potential application for virtual reality and augmented reality is emphasized. © 2017 Optical Society of America

The recent rapid growth of near-eye virtual reality (VR) and augmented reality (AR) has accelerated the demand for a display system with high angular resolution and a large field of view (FOV). To achieve a FOV of around 100°, the current angular resolution of commercial VR displays lies at around 6 arcmin, while the acuity of a normal person with 20/20 vision is about 1 arcmin. As a result, clear pixels (also known as the screen door effect) can be observed by most users, rendering it difficult to achieve a fully immersive experience in the virtual contents. To enhance resolution at a fixed FOV, tremendous efforts have been spent to increase the number of pixels on small display panels up to 3 k by 3 k for each eye [1–6]. However, to achieve 1 arcmin resolution, a display with 6 k by 6 k pixels for each eye will eventually be needed. Such a high pixel density would post challenges not only to the device fabrication, but also to driving electronics because of the much shorter addressing time for each scan line. For a transmissive liquid crystal display (LCD), this also results in smaller aperture ratio and lower transmittance.

To address this issue, instead of increasing the number of pixels, several efforts [7–11] have been developed to shift the image by a fraction of the pixel width and computationally generate corresponding images to achieve high resolution. These earlier studies mainly focus on cameras or projectors. By exploiting a mechanical image shifter to slightly shift the

image in temporal domain, Allen and Ulichney demonstrated a high-resolution projection display [7]. Such a mechanical image shifter works well for projectors, but for near-eye displays this will inevitably increase the form factor and, moreover, it is undesirable for the user to feel the vibration from the wearable device. To avoid mechanical movement, another approach is to look into optically overlaying or stacking displays [8–12]. While it provides enhanced resolution, using multiple panels often results in complicated system integration and decreased transmittance.

In this Letter, we propose a simple method by exploiting fast-switching Pancharatnam–Berry deflectors (PBDs) as non-mechanical image shifters to increase the display resolution. By turning on and off the PBD, synchronizing with computationally generated sub-frame images, we demonstrated an enhanced resolution with minimal increase in system complexity.

A PBD is a single-order phase grating with high diffraction efficiency [13–19]. The structure of PBD consists of patterned half-wave plates with in-plane variation in the crystal axis, denoted as $\phi(x, y)$. With a circularly polarized input light, a Jones calculus can be established as [13]

$$J'_\pm = \frac{1}{\sqrt{2}} \begin{bmatrix} \cos 2\phi & \sin 2\phi \\ \sin 2\phi & -\cos 2\phi \end{bmatrix} \begin{bmatrix} 1 \\ \pm i \end{bmatrix} = \begin{bmatrix} 1 \\ \mp i \end{bmatrix} e^{\pm 2i\phi}. \quad (1)$$

Equation (1) indicates that the angle of crystal axis, $\phi(x, y)$, will translate into a wavefront delay of 2π for a circularly polarized input light. For example, in Fig. 1(a), when the crystal axis rotates by 180° spatially along the x-axis in a linear fashion (denoted as $P/2$), the wavefront delay for a circular input light also changes linearly and reaches 360° (2π). The mathematical formulation of the in-plane crystal axis $\phi(x, y)$ can be expressed as

$$\phi(x, y) = (2\pi/P)x. \quad (2)$$

The linear wavefront delay is then simply $2\phi(x, y) = \frac{4\pi}{P}x$. As it provides a linear wavefront delay, the PBD is a high-efficiency phase grating with only one diffraction order for a circularly polarized light. A PBD deflects light through diffraction and the deflection angle (θ) can be described by

$$P/2 = \lambda/\sin\theta. \quad (3)$$

Such a beam deflection can be exploited to shift the display pixels. Let us assume that a commercial VR headset has an
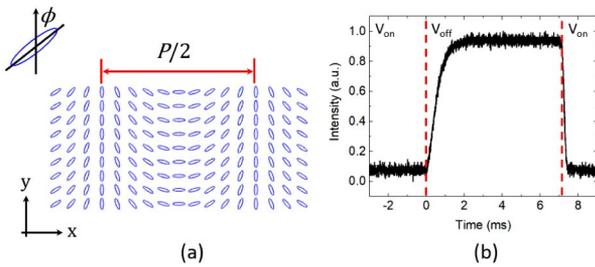
Fig. 1. (a) Top view of the LC director (i.e., optical axis, ϕ) distribution in a PBD, where the LC director rotates by 180° is defined as half a period, $P/2$. Inset: the definition of optical axis ϕ where the LC molecules are represented as an ellipse, and the longer axis of the ellipse is the optical axis. (b) Measured turn-on time is 0.4 ms, and the turn-off time is 0.8 ms.

angular resolution of 6 arcmin. To shift half a pixel in angular space diagonally (along 45°), a deflection of $3/\sin(45°) \cong 4.2$ arcmin will be needed. Because the required deflection angle is small, the difference in deflection angle for different visible wavelengths can be neglected.

From Eq. (1), the wavefront delay has an opposite sign for the left circularly polarized (LCP) and right circularly polarized (RCP) lights. This indicates that the PBD is polarization dependent. If the LCP input is deflected by 4.2 arcmin, then the RCP will be deflected by –4.2 arcmin. Therefore, in many cases, it is desirable to adapt a display with circularly polarized output light.

To demonstrate feasibility, in experiment, we employed an electrically switchable PBD. In a voltage-on state, the nematic liquid crystal (LC) directors are reoriented to be vertical to the substrate. As a result, the incident light experiences no phase change. In this voltage-on state, the beam is not deflected, and we refer to this case as the original state. When the voltage is released, the LC directors follow the surface alignment, as shown in Fig. 1(a), and the light will be deflected. We refer to this state as the shifted state.

A fast-switching PBD is needed to shift the pixels between the original state (denoted as sub-frame 1) and the shifted state (denoted as sub-frame 2). This shift will allow enhanced resolution through computationally calculating the correct image to be displayed for each sub-frame.

In experiment, we fabricated a fast-switching PBD by interference exposure. The cleaned indium-tin-oxide glass substrates were first spin-coated with a thin photoalignment layer (PAAD-72 from BEAM Company [20]). The substrates were sealed to form a 1.8 μm cell gap. A Mach–Zehnder interferometer ($\lambda = 442$ nm, He-Cd laser) was set up to expose the sealed sample with two opposite circularly polarized beams from each arm interfering on the sample at an angle of 0.053° (3.2 arcmin). After exposure for a dosage of 3 J/cm², we infiltrated a low-viscosity LC mixture UCF-PB1 into the cell. The chemical composition of UCF-PB1 is similar to that reported in [21], and its physical properties are $\Delta n = 0.14$ at $\lambda = 532$ nm, dielectric anisotropy $\Delta\varepsilon = 3.0$, and visco-elastic constant $\gamma_1/K_{11} = 3.3$ ms/μm² at 22°C. The LC cell has a half-period of 475 μm (across which the crystal axis rotates by 180°), resulting in a deflection angle of 3.85 arcmin at $\lambda = 532$ nm [see Eq. (3)] at the voltage-off state. Such a deflection angle is chosen in order to shift diagonally a 5.4 arcmin pixel

by a half-period. By applying a voltage of 7 V_{rms} (voltage-on state), the LC directors are reoriented perpendicular to the substrates, becoming optically transparent so that the incident light does not deflect.

To measure the switching time of our PBS, we sent a He–Ne laser beam ($\lambda = 633$ nm) to the PBD sample at normal incidence, and positioned a photodetector and an iris at 2 meters away from the PBD. When the voltage on the PBD was turned off, the laser beam was deflected and received by the detector. When the voltage was turned on, the laser beam was not deflected so that it was blocked by the iris. Due to the low viscosity of the employed LC material and thin cell gap, the switching time between the zeroth order and first order was less than 1 ms, as shown in Fig. 1(b).
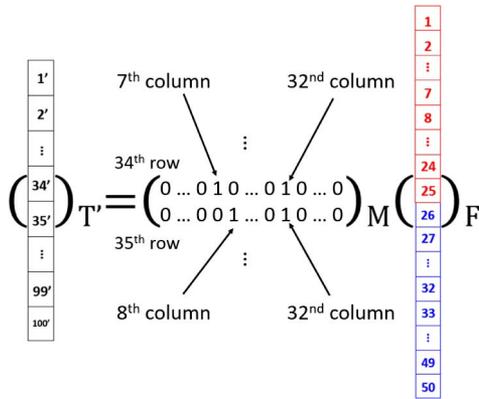
To generate enhanced resolution, a display panel was synchronized to the PBD. As the PBD is switched to the original state, sub-frame image 1 is displayed on the panel, and as the PBD is switched to the shifted state, sub-frame image 2 is displayed on the panel. These two computationally generated sub-frame images 1 and 2 displayed on original and shifted displays are added in brightness when perceived by human eyes when the switching rate is sufficiently high.

The system setup is shown in Fig. 2(a); it consists of a display magnified with a lens and then shifted by a PBD. The outgoing light from the display panel is circularly polarized. Let us illustrate the working principle of pixel shifting with some pixels, as Fig. 2(a) depicts. The output ray is denoted as red lines. As it traverses through the PBD at voltage-on state, the light is not deflected, and the original display is observed. As the PBD switches to the voltage-off state, the light is deflected and is denoted as blue rays. Under such a condition, the observer sees effectively the shifted pixels as coming from the *dashed* blue lines. The shifting occurs for all pixels and, therefore, a PBD can be exploited as an image shifter.

To illustrate the computational method for calculating correct sub-frame images, we adopt a linear least-square method as described below, although other methods [7] may also be used. Let us assume a low-resolution physical display panel with 5×5 pixels, as shown in Fig. 2(b). The original display with square pixels is plotted in red, and the shifted display pixels are plotted in blue. Pixels 1 through 25 are labeled for the original display, while 26 through 50 are labeled for the shifted display. We express the pixels on sub-frames 1 and 2 in sequence as a column vector $\mathbf{F}_{50\times1}$ [see the red and blue indices in Fig. 2(b)]. The combined image due to the fast-switching PBD forms a high-resolution grid (10×10) with pixels labeled 1′ through
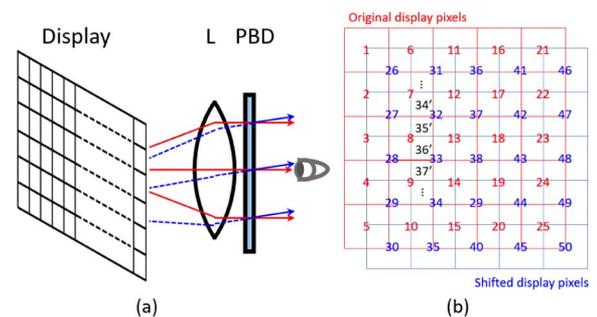
Fig. 2. (a) Experimental setup for enhancing resolution with a PBD. (b) Pixel illustration of the original display (sub-frame 1), the shifted display (sub-frame 2), and the combined pixels.

$$\begin{pmatrix} 1' \\ 2' \\ \vdots \\ 34' \\ 35' \\ \vdots \\ 99' \\ 100' \end{pmatrix}_{T'} = \begin{pmatrix} 0 \ldots 0\,1\,0 \ldots 0\,1\,0 \ldots 0 \\ 0 \ldots 0\,0\,1 \ldots 0\,1\,0 \ldots 0 \end{pmatrix}_{M} \begin{pmatrix} 1 \\ 2 \\ \vdots \\ 7 \\ 8 \\ \vdots \\ 24 \\ 25 \\ 26 \\ 27 \\ \vdots \\ 32 \\ 33 \\ \vdots \\ 49 \\ 50 \end{pmatrix}_{F}$$

7th column, 32nd column, 34th row, 35th row, 8th column, 32nd column

Fig. 3. Illustration of the matrix form of adding a low-resolution time-multiplexed display (**F**) to yield the combined image (**T′**). The correlation matrix **M** essentially performs an addition operation. For example, the 34th row of **M** adds element #7 and #32 in **F** to yield element #34′ in **T′**. Therefore, only the 7th and 32nd elements in the 34th row are 1, and all other are zero.

100′, and we express it as a column vector $\mathbf{T}'_{100\times1}$ [see the black indices in Fig. 2(b)]. The temporal pixel shift by switching of the PBD results in an additive brightness, as the human eye integrates the two sub-frames. From Fig. 2(b), we can establish this additive correlation between the combined image ($\mathbf{T}'_{100\times1}$) and sub-frames 1 and 2 ($\mathbf{F}_{50\times1}$). For example, pixels #7 and #32 jointly decide pixel #34′, i.e., brightness of #34′ = #7 + #32, and #35′ = #8 + #32, and so on. This additive correlation is then expressed as a correlation matrix $\mathbf{M}_{100\times50}$.

Therefore, as illustrated in Fig. 3, the relation between combined image (**T′**) and sub-frames 1 and 2 (**F**), can be written as

$$\mathbf{T}'_{4N\times1} = \mathbf{M}_{4N\times2N}\mathbf{F}_{2N\times1}. \tag{4}$$

Here we denote the pixel number of the low-resolution panel by N ($N = 5 \times 5 = 25$ in this illustration). Equation (4) simply states an additive relation between **F** and **T′**; i.e., the brightness of every pixel in the combined image is the sum of two relevant low-resolution pixels; the correlation matrix, **M**, essentially performs an addition. After sorting out the correct form of **M**, we can input a high-resolution target image to calculate the correct images to be displayed in the low-resolution sub-frames 1 and 2 (i.e., vector **F**).

Assume we have a high-resolution target image (at twice the resolution of the low-resolution physical display panel) to be displayed, denoting the high-resolution target image as vector $\mathbf{T}_{100\times1}$. We need to find the correct images to display for each sub-frame (vector **F**), which minimizes the difference between the combined display image (**T′**) and the high-resolution image (**T**):

$$\arg\min_{\mathbf{F}} \frac{1}{2} \|\mathbf{M}_{4N\times2N}\mathbf{F}_{2N\times1} - \mathbf{T}_{4N\times1}\|_2^2. \tag{5}$$

This is the standard linear least-square problem, and there are several methods [22] for solving this type of problem. Here we use the built-in Matlab function lsqlin. **M** (correlation matrix) and **T** (target high-resolution image) are known and, through lsqlin solver, finally, we can obtain **F**, which is the two sub-frame images to be displayed on the original and shifted low-resolution panel. The red, green, and blue channels are calculated separately and then combined to obtain color images. Note that a constraint for **F** was

applied for an lsqlin solver requiring that every element be larger than 0 for there is no negative brightness. In addition, note that in the computation, the pixel values are first decoded by a power of 2.2 (gamma correction) to get relative brightness, and then after solving the least-squares problem, encoded by a power of 1/2.2. Otherwise, the direct addition of pixel values yields false results (since the eye sees additive brightness, not additive pixel values).

This computation solves an overdetermined problem with 4N constraints and 2N variables, where N is the total number of pixels on the physical low-resolution panel. This means that the improvement in resolution will be less for a fully randomized image ("white noise" image). Yet, in regular images, adjacent pixels usually have similar pixel values, which relieves the constraint and allows better results that are closer to the target high-resolution image. Also, it is not necessary to perform computation on all pixels since the high-resolution region in human eye actually restricts to only a very small FOV close to the fovea.

The computed images, using a "Siemens star" as an example, are shown in Figs. 4(a) and 4(b); they were used as sub-frame images 1 and 2, respectively. In Fig. 5, the image was taken through the setup, as explained in Fig 2(a). Since current commercially available smartphone-sized displays do not have sufficiently high refresh rates, a 144 Hz monitor (VG248, ASUS) was used in this experiment. A bi-convex lens (focal length = 10 cm) was chosen to magnify the display panel to mimic commercial VR headsets with an angular size of 5.4 arcmin for each pixel. A quarter-wave plate was placed after the lens to turn linearly polarized display light into circular polarization. The PBD sample was placed adjacent to the quarter-wave plate to shift the display by half a pixel diagonally. A voltage of 7 V_{rms} (1 kHz square wave) was applied and released at 72 Hz to switch between the original display and shifted display. (The PBD is on for 1/144 s and off for 1/144 s, repeatedly.) The on-off cycle of the PBD was synchronized with the display panel, and the computed sub-frame image 1 [e. g., Fig. 4(a)] was displayed during the PBD-on state, while sub-frame image 2 was displayed during the PBD-off state [e.g., Fig. 4(b)]. A camera (Canon EOS Rebel T5i) was placed after the PBD to capture the enhanced images.

Compared to the image displayed at original resolution [Fig. 5(a)], we can clearly see the enhancement in resolution, especially for those regions with curved or sloped contours, as shown in Fig. 5(b). The upper image is the example of a "Siemens star"; it is clearly seen that the pixels in the original resolution are much less visible than those in the enhanced resolution, and the discontinuous boundary with pixel jumps is smoother after enhancement. The lower image is an example of a lady. Similarly, the pixels are less discernible, and the eye of the lady becomes smoother after enhancement. Note that the
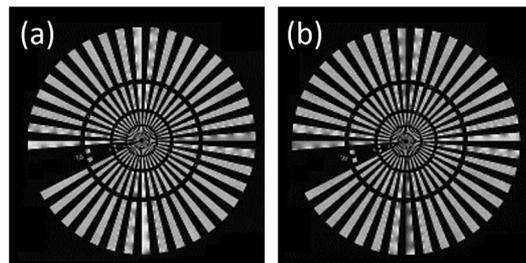
Fig. 4. Computed images for (a) sub-frame 1 and (b) sub-frame 2.

(a) Original   (b) Enhanced
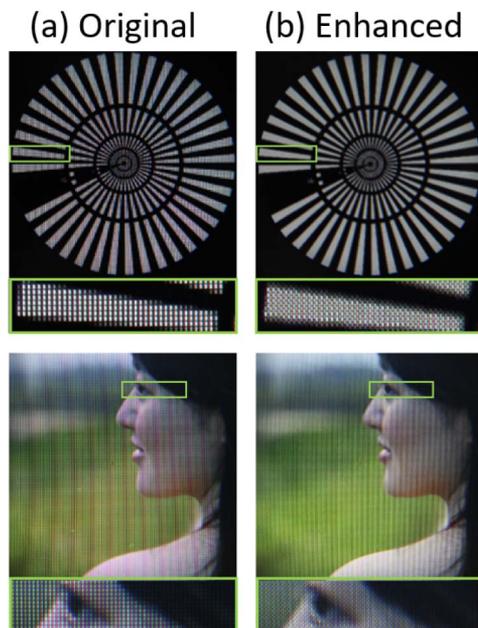
Fig. 5. Images captured through a camera for (a) the original resolution and (b) the enhanced resolution for (upper) a "Siemens star" resolution target and (lower) a lady. The green rectangles enclose the magnified regions shown in the pictures. Note that the visible strips are a moiré pattern from the spatial interference of camera and display pixels, and are not visible when directly seen with human eyes.

strips in the picture were a moire pattern resulting from spatial interference of camera and display pixels and are not visible when directly seen with human eyes. It is noticeable, however, that the color representation and brightness are different after enhancement. This shift in color can be corrected by taking into account the efficiency difference of the PBD at different wavelengths [13] and calibrating the correlation matrix **M** accordingly for the RGB channels.

It should be mentioned that as a time-multiplexing display device, potential image quality degradation may occur due to eye movement. When no eye movement is involved, the two sub-frames imaged on the retina are well defined, as discussed above. However, when eye movement is sufficiently fast, the sub-frames may not map to the ideal location on the retina, which could result in blurred artifacts.

It is also important to note that the addition-based correlation matrix results in a subtle decrease in brightness. This is because the brightness of a pixel was distributed into two sub-frames with only half the frame time. For example, in Fig. 2(b), assuming a high-resolution image at pixel #34′ has a pixel value of 230 (a brightness of $230^{2.2}$ in arbitrary units, [a.u.]), and it is computed with Eq. (5) to have the pixel values of #7 being 200 and #32 being 125 (such that the summed brightness being $200^{2.2} + 125^{2.2} \cong 230^{2.2}$ a.u.) each for 1/144 s; then the integrated brightness over time is only half (integrated brightness being $1/144 \times 200^{2.2} + 1/144 \times 125^{2.2}$ in arbitrary units), compared to the case using an actual high-resolution physical panel with pixel being at 230 for 1/72 s (integrated brightness being $1/72 \times 230^{2.2}$ in arbitrary units), assuming the high-resolution physical panel has the same

maximum brightness as the low-resolution physical panel. It should be noted that even though the effective brightness is reduced, the optical efficiency remains the same, because the loss in brightness is only a result of computational rendering instead of extra optical absorption. This reduction in brightness is accounted for in the comparison in Fig. 5 by reducing the intensity by half for figures with original resolution [Fig. 5(a)].

In conclusion, using a PBD as a pixel shifter, the effective display resolution can be enhanced. This method allows simple integration to a near-eye display device, either AR or VR, and only minimally increases the form factor. It can be integrated to different display panels such as transmissive LCD, reflective LC-on-silicon, reflective digital light processing, and emissive organic light emitting diode display, with a minimal refresh rate of 120 Hz.

REFERENCES

1. T. Matsuo, Y. Kanzaki, H. Matsukizono, A. Oda, S. Kaneko, N. Ueda, Y. Kataoka, H. Shishido, K. Takahashi, S. Yamazaki, K. Okazaki, and J. Koezuka, SID Int. Symp. Dig. Tech. Pap. **47**, 1029 (2016).
2. S. Kawashima, H. Shishido, S. Oshita, S. Yoshitomi, A. Yamashita, T. Ishitani, A. Sato, M. Jincho, Y. Shima, M. Katayama, and S. Yamazaki, SID Int. Symp. Dig. Tech. Pap. **48**, 242 (2017).
3. H. S. Lee, S. Jang, J. Noh, H. Jeon, B.-S. Choi, Y. M. Jeon, K. Song, J. Song, H. Y. Chu, and S. Kim, SID Int. Symp. Dig. Tech. Pap. **48**, 403 (2017).
4. W. P. Bleha and L. A. Lei, Proc. SPIE **8736**, 87360A (2013).
5. A. Ghosh, E. P. Donoghue, I. Khayrullin, T. Ali, L. Wacyk, K. Tice, F. Vazan, O. Prache, Q. Wang, L. Sziklas, D. Fellowes, and R. Draper, SID Int. Symp. Dig. Tech. Pap. **47**, 837 (2016).
6. K. Kimura, Y. Onoyama, T. Tanaka, N. Toyomura, and H. Kitagawa, J. Soc. Inf. Disp. **25**, 167 (2017).
7. W. Allen and R. Ulichney, SID Int. Symp. Dig. Tech. Pap. **36**, 1514 (2005).
8. F. Heide, D. Lanman, D. Reddy, J. Kautz, K. Pulli, and D. Luebke, ACM Trans. Graph. **33**, 60 (2014).
9. C. Jaynes and D. Ramakrishnan, in *IEEE International Workshop on Projector-Camera Systems* (2003), pp. 354–356.
10. Y. Kusakabe, M. Kanazawa, Y. Nojiri, M. Furuya, and M. Yoshimura, J. Soc. Inf. Dis. **16**, 383 (2008).
11. Y. Kusakabe, M. Kanazawa, Y. Nojiri, M. Furuya, and M. Yoshimura, Proc. SPIE **7241**, 72410Q (2009).
12. B. Sajadi, M. Gopi, and A. Majumder, ACM Trans. Graph. **31**, 1 (2012).
13. Y. H. Lee, G. Tan, T. Zhan, Y. Weng, G. Liu, F. Gou, F. Peng, N. V. Tabiryan, S. Gauza, and S. T. Wu, Opt. Data Process. Storage **3**, 79 (2017).
14. S. Pancharatnam, Proc. Indian Acad. Sci. A **44**, 247 (1956).
15. M. V. Berry, Proc. R. Soc. London Ser. A **392**, 45 (1984).
16. E. Hasman, V. Kleiner, G. Biener, and A. Niv, Appl. Phys. Lett. **82**, 328 (2003).
17. H. Chen, Y. Weng, D. Xu, N. V. Tabiryan, and S.-T. Wu, Opt. Express **24**, 7287 (2016).
18. H. Cheng, A. K. Bhowmik, and P. J. Bos, Appl. Opt. **54**, 10035 (2015).
19. K. Gao, C. McGinty, H. Payson, S. Berry, J. Vornehm, V. Finnemeyer, B. Roberts, and P. Bos, Opt. Express **25**, 6283 (2017).
20. N. Tabiryan, D. Roberts, D. Steeves, and B. Kimball, Photon. Spectra **51**, 46 (2017).
21. Z. Luo, F. Peng, H. Chen, M. Hu, J. Li, Z. An, and S. T. Wu, Opt. Mater. Express **5**, 603 (2015).
22. T. F. Coleman and Y. Li, SIAM J. Optim. **6**, 1040 (1996).